Epitaxy of $CoSi_x$ ($1<x<2$) silicides on Si(111) studied by photoemission and extended x-ray-absorption fine-structure techniques

C. Pirri, S. Hong, M. H. Tuilier, P. Wetzel, and G. Gewinner
Laboratoire de Physique et de Spectroscopie Electronique Faculté des Sciences et Techniques 4, rue des Frères Lumière 68093 Mulhouse Cédex, France

R. Cortès
Laboratoire pour l'Utilisation du Rayonnement Electromagnétique Université de Paris-Sud, 91405 Orsay Cédex, France
(Received 28 April 1995)

Electronic and structural properties of epitaxial $CoSi_x$ layers have been investigated by means of core-level and valence-band photoemission, x-ray photoelectron diffraction, and extended x-ray-absorption fine-structure (EXAFS) experiments. $CoSi_x$ layers of various x compositions have been grown on silicon by low rate Co and Si co-deposition onto room-temperature Si(111) substrates, with film thicknesses ranging from 30 to 100 Å. Photoemission shows substantial differences in valence and core-level spectra with respect to those of stable fluorite-type $CoSi_2$ and ε-CoSi and indicate that well-defined metastable phases are formed. In particular, core-level photoemission experiments performed with a monochromatized x-ray source show large Si $2p$ binding-energy shifts ($\sim$0.4 eV) in the room-temperature deposited $CoSi_x$ ($1<x<2$), with respect to stable ε-CoSi and CaF_2-type $CoSi_2$. X-ray photoelectron diffraction as well as extended x-ray-absorption fine-structure measurements suggest that these pseudomorphic phases have a cubic structure, over a wide composition range. EXAFS measurements reveal that Co atoms are coordinated with eight Si atoms with a bond length of $\sim$2.33 Å and with Co atoms with bond lengths in the 2.67–2.68 Å range. Such short Co-Co bond lengths show that the structure is definitively different from the stable CaF_2-type $CoSi_2$, even at the $CoSi_2$ composition. All experimental data indicate that $CoSi_x$ silicides crystallize in a cubic lattice close to that of pseudomorphic $FeSi_x$ silicides, namely, a CsCl-type derived structure.

I. INTRODUCTION

The growth of ordered metastable phases on metallic or semiconducting substrates is of great importance, since they could exhibit physical properties, not encountered in bulk materials. Recent accounts for the growth of metastable materials on Si(111) have been given for the Fe silicide-Si system. The Fe silicide-silicon system is a prototypical system with respect to these considerations, since several unusual Fe silicide phases, i.e., pseudomorphic phases, can be stabilized by epitaxy on Si(111). In particular, the formation of a metallic FeSi phase, with a CsCl-type structure using the molecular-beam technique, has been reported (the stable ε-FeSi phase crystallizes in a simple cubic $B20$-type lattice).[1] Thin $FeSi_2$ layers were found to crystallize in three metastable structures: a cubic CsCl-type FeSi derived structure,[2–5] an α-$FeSi_2$ derived structure,[6,7] and a fluorite (CaF_2-type) structure.[8–10] Furthermore, it was shown that Fe silicides with a composition between FeSi and $FeSi_2$ can also be grown on Si(111) with a CsCl-type structure.[1–3,5] The stable ε-FeSi phase has a lattice misfit of -4.7%, with respect to Si. The $FeSi_2$ phase exists in two forms in the bulk phase diagram: the orthorhombic β-$FeSi_2$ phase, stable up to 920 °C and the quadratic α-$FeSi_2$, which exists only above 920 °C. β-$FeSi_2$ crystallizes in an orthorhombic structure with lattice parameters $a=9.863$ Å, $b=7.791$ Å, and $c=7.833$ Å.[11] Epitaxy of β-$FeSi_2$ on Si(111) has been observed either with β-$FeSi_2(100)\|Si(111)$ or with β-$FeSi_2(110)\|Si(111)$. In both cases, the lattice misfit is of $\sim 5-6$ %. It seems that the rather large mismatch between bulk Fe silicides (ε-FeSi and β-$FeSi_2$) lattices as well as the very different atomic arrangement in the (111) planes of stable Fe silicide and Si make thin silicide layers adopt a crystal structure, which is better lattice matched to the substrate. The formation of a CsCl-type CoSi, epitaxially grown on Si(111) at room temperature has been reported more recently.[12] The stable CoSi phase, namely, ε-CoSi, also crystallizes in a simple cubic $B20$-type structure, with a lattice misfit of -5.6%, with respect to Si.[11] As opposed to bulk ε-CoSi, ε-FeSi, and β-$FeSi_2$ silicides, the mismatch between stable CaF_2-type $CoSi_2$ and Si is rather small (-1.2%) and the atomic arrangement in the $CoSi_2(111)$ and Si(111) planes is very similar. Nevertheless, we show in this paper, by means of x-ray photoelectron diffraction (XPD), extended x-ray-absorption fine structure (EXAFS), and valence-band and core-level photoemission, that a metastable $CoSi_2$ phase forms indeed upon room-temperature co-deposition of Co and Si on Si(111). Epitaxy of $CoSi_2$ on Si(111) at room temperature has already been reported, but no investigation of its crystallographic structure was done at that time.[13,14] This phase is stable up to $\sim 400-450$ °C. Furthermore, we have found that epitaxial $CoSi_x$ silicides, with $1<x<2$, can be also grown on Si(111). Experimental data show that they have a crystallographic, as well as electronic structure very similar to that of the CsCl-type FeSi derived $FeSi_x$ silicides grown on Si(111).

II. EXPERIMENTAL PROCEDURE

Epitaxial $CoSi_x$ silicides with composition $1<x<2$ were prepared on Si(111) in a UHV system, with a base pressure

of 7×10^{-11} mbar. Co and Si were evaporated in the 1–2 Å/min rate range from boron nitride and carbon crucibles, respectively. The silicide composition was controlled by means of calibrated quartz microbalances, which measured the Co and Si fluxes independently, during the silicide growth. Prior to $CoSi_x$ deposition, the Si(111) substrates were cleaned by heating the sample up to ~900–950 °C. This procedure leads to a well-ordered Si(111) surface, as attested by a sharp 7×7 low-energy electron-diffraction (LEED) reconstruction. Absence of oxygen or carbon on the surface was checked by x-ray photoelectron spectroscopy. The $CoSi_x$ layers were grown in two steps. First, a 9-Å-thick $CoSi_2$ was co-deposited onto the clean Si(111) surface and subsequently annealed at 550 °C. A well-ordered $CoSi_2$ layer is achieved in this way, as attested by a well-defined 1×1 LEED pattern and sharp confinement states observed at ~0.5 eV on the ultraviolet photoemission spectroscopy spectrum.[15,16] Second, 30–100-Å-thick $CoSi_x$ layers were deposited onto such substrates maintained at a temperature lower than 100 °C. In this paper, such silicides films are called ''room-temperature grown,'' as opposed to stable Co-silicides phases achieved by anneals at temperatures above 300 °C, typically.

Photoemission measurements were carried out using a Leybold Heraeus EA 200 spectrometer, equipped with a high power (1600 W) unmonochromatized x-ray source (photon energy $\hbar\omega=1486.6$ eV) used for XPD measurements and a monochromatized x-ray source (photon energy $\hbar\omega=1486.6$ eV) used for higher-resolution valence-band and core-level measurements. The photoelectrons were analyzed using a hemispherical energy analyzer (150 mm in radius), with a 50-meV energy resolution and an 18-channel multidetection assembly. The overall energetic resolution, using the monochromatized Al $K\alpha$ source, was about 0.5 eV. The two-stage electron lens at the entry of the electron analyzer allowed a tunable angular resolution in the $\pm1°$ and $\pm8°$ range. The acceptance angle of the analyzer was set to $\pm8°$ for high-energy-resolution core-level measurements and to $\pm1°$ for XPD measurements. Co $2p_{3/2}$ and Si $2p$ core lines were recorded at kinetic energy $E_c=706$ and 1388 eV, respectively.

After photoemission measurements, a 20-Å-thick protective amorphous Si capping layer was deposited onto the silicide films. EXAFS measurements were performed at the Laboratoire pour l'Utilisation du Rayonnement Electromagnétique at Orsay on the XAS 2 beam line of the DCI storage ring. The incident radiation was monochromatized using a Si(111) plane two-crystal spectrometer. The beam line was equipped with a mirror at glancing incidence for the harmonic rejection. The variation of the x-ray-absorption coefficient was measured above the K edge of cobalt (7709 eV) at RT in the fluorescence mode. A detailed description of the data collection is given in Ref. 5.

III. RESULTS AND DISCUSSION

The $CoSi_x$ silicides are epitaxial after deposition, as attested by a 1×1 LEED pattern. For compositions close to CoSi, the LEED pattern reveals additional spots arising from electron diffraction on [101] oriented facets. The presence of these additional LEED spots depends critically on the film thickness. Their observation begins above 30 Å and they dominate the LEED pattern for thicknesses typically higher than 100 Å. In any case, the 1×1 LEED pattern is slightly improved by mild annealing up to temperatures ranging from 300 °C (Co-rich silicide) to ~400 °C (Si-rich silicides). Anneals at higher temperatures induce phase transitions towards stable phases. Pseudomorphic CoSi is completely transformed into the stable ε-CoSi phase upon annealing at 350–400 °C. At this stage, the 1×1 LEED pattern disappears, leaving only a strong diffuse background. Pseudomorphic $CoSi_2$ is transformed into the stable epitaxial CaF_2-type $CoSi_2$ phase upon annealing at ~500 °C. This latter phase also exhibits a 1×1 LEED pattern. These phase transitions are clearly evidenced by valence-band spectra measurements. Figure 1 shows valence-band spectra taken with the monochromatized x-ray source on the Co silicides below and above the phase transition. Pseudomorphic CoSi and $CoSi_2$ valence bands are mainly composed of a broad peak centered at ~1.5 and 1.7 eV binding energy, respectively. Additional weak structures are observed at higher binding energies, which extend to about 5-eV binding energy. The CoSi spectrum is in good agreement with that published in Ref. 12. It evolves into a spectrum dominated by a double peak at 1.1- and 2.2-eV binding energy, upon annealing at 400 °C. This double peaked shape is characteristic of monosilicides crystallizing in the cubic $B20$ structure, such as ε-FeSi and ε-CoSi.[17–19] The CaF_2-type $CoSi_2$ valence-band spectrum of Fig. 1 is characterized by two main structures located at ~1.5- and 3.5-eV binding energy, arising from nonbonding and bonding states, respectively.[20,21] For compositions in between, $CoSi_x$ evolves into a mixed phase composed of

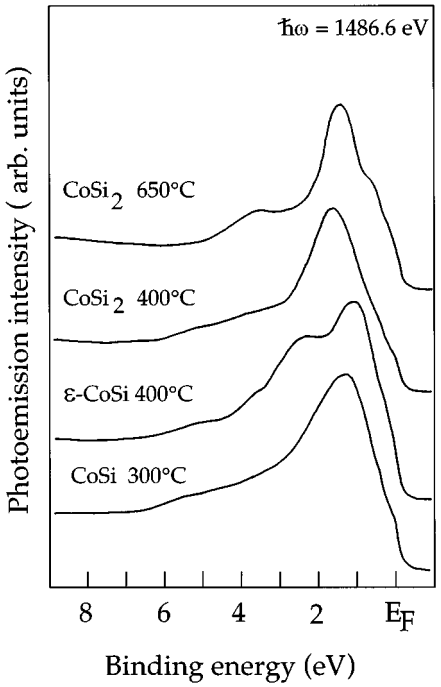

FIG. 1. Valence-band spectra collected at normal electron emergence for stable CaF_2-type $CoSi_2$, ε-CoSi and pseudomorphic CoSi and $CoSi_2$ silicides. Spectra were recorded using a monochromatized Al $K\alpha$ source at a photon energy of 1486.6 eV.

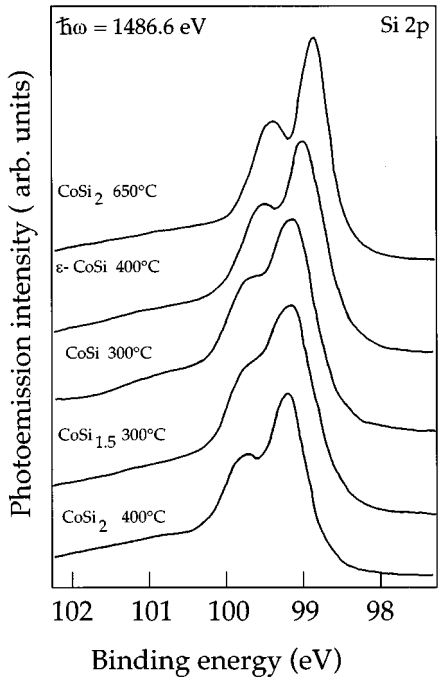

FIG. 2. Si $2p$ spectra collected at normal electron emergence for stable CaF_2-type $CoSi_2$, ε-CoSi and pseudomorphic CoSi, $CoSi_{1.5}$, and $CoSi_2$ silicides. Spectra were recorded using a monochromatized Al $K\alpha$ source at a photon energy of 1486.6 eV.

ε-CoSi and fluorite-type $CoSi_2$, upon annealing above 500 °C.

At compositions close to CoSi, the distinction between pseudomorphic and stable phases is clear, on the basis of LEED observations. For compositions close to $CoSi_2$, LEED exhibits a 1×1 pattern for both pseudomorphic and stable phases. Hence, it must be shown that these samples are composed of a single phase and not a mixture of phases that include an appreciable amount of CaF_2-type $CoSi_2$. Information about this crucial point can be gained by core-level Si $2p$ and Co $2p_{3/2}$ measurements. Figure 2 shows the Si $2p$ lines measured on the room-temperature grown $CoSi_x$, subsequently annealed in the 300–400 °C range. These spectra are presented along with that of stable CaF_2-type $CoSi_2$. Co $2p_{3/2}$ lines measured on $CoSi_x$ and CaF_2-type $CoSi_2$ silicides are shown in Fig. 3. The photoemission spectra of Figs. 2 and 3 were obtained with monochromatized Al $K\alpha$ radiation $\hbar\omega$=1486.6 eV and were collected at normal electron emergence. The silicide thickness is large enough (90 Å) to avoid substrate contribution to the signal and to minimize surface effects. Figure 2 shows that metastable silicide Si $2p$ lines are substantially shifted towards higher binding energies, with respect to clean Si(111), ε-CoSi or fluorite-type $CoSi_2$. Si $2p$ lines are shifted by about 0.35 eV, with respect to CaF_2-type $CoSi_2$ and by about 0.20 eV, with respect to ε-CoSi. At the $CoSi_2$ and $CoSi_{1.5}$ compositions, the Co $2p_{3/2}$ lines lie at the same binding energy as the fluorite $CoSi_2$ or ε-CoSi ones. Improvement of the silicide crystallinity upon annealing is characterized by an appreciable decrease of their full width at half maximum. The stability of the as-deposited $CoSi_2$ phase versus annealing temperature has been examined. Figure 4 shows the Si $2p$ line evolution of a room-temperature deposited $CoSi_2$ layer, as a function of annealing temperature (15-min anneals). After co-deposition the Si $2p$ line is broader and shifted by ~0.40 eV, with respect to that

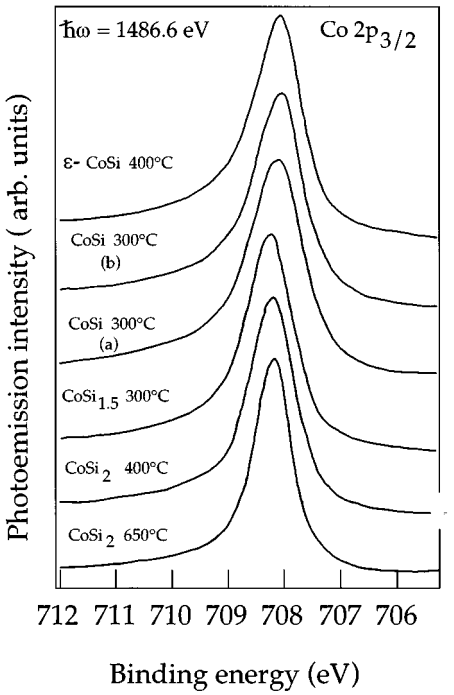

FIG. 3. Co $2p_{3/2}$ spectra collected at normal electron emergence for stable CaF_2-type $CoSi_2$, ε-CoSi and pseudomorphic CoSi, $CoSi_{1.5}$, and $CoSi_2$ silicides. Spectra were recorded using a monochromatized Al $K\alpha$ source at a photon energy of 1486.6 eV.

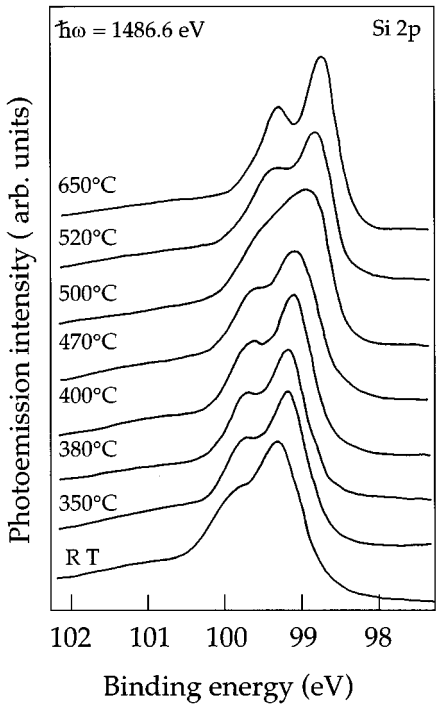

FIG. 4. Si $2p$ spectra collected at normal electron emergence for 90-Å-thick room-temperature co-deposited $CoSi_2$ silicide versus annealing temperature. Spectra were recorded using a monochromatized Al $K\alpha$ source at a photon energy of 1486.6 eV.

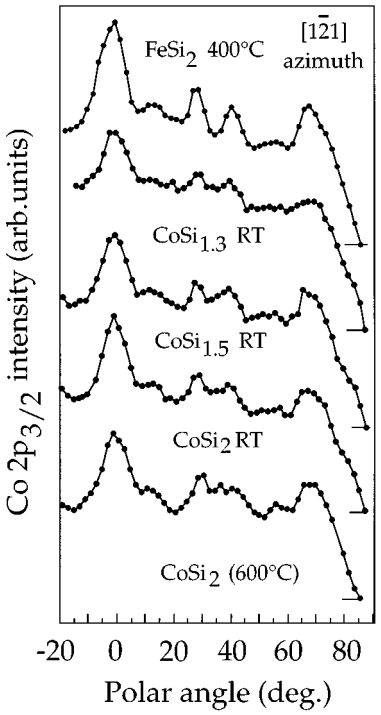

FIG. 5. Experimental polar-angle scans of Co $2p_{3/2}$ emission for 90-Å-thick pseudomorphic $CoSi_{1.3}$, $CoSi_{1.5}$, and $CoSi_2$, CaF_2-type $CoSi_2$ and pseudomorphic $FeSi_2$ silicides, epitaxially grown on Si(111), along the [121] azimuth of the Si(111) substrate. The polar angle $\theta=0°$ corresponds to emission normal to the sample.

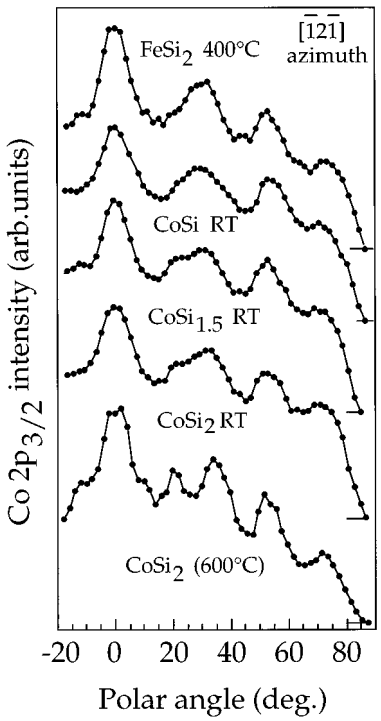

FIG. 6. Experimental polar-angle scans of Co $2p_{3/2}$ emission for 90-Å-thick pseudomorphic $CoSi_{1.5}$ and $CoSi_2$, CaF_2-type $CoSi_2$ and pseudomorphic $FeSi_2$ silicides, epitaxially grown on Si(111), along the [121] azimuth of the Si(111) substrate. The polar angle $\theta=0°$ corresponds to emission normal to the sample.

of the CaF_2-type $CoSi_2$ (topmost spectrum), where the Co occupies a single well-defined crystallographic site. Upon annealing at 350 °C, a slight binding energy decrease is observed along with better resolved Si $2p_{1/2}$-Si $2p_{3/2}$ spin-orbit split components. The Si $2p$ line binding energy remains rather unchanged up to ~450 °C. At this stage, the Si $2p$ line has a full width at half maximum comparable to that of fluorite $CoSi_2$. The transition towards stable CaF_2-type $CoSi_2$ mainly starts at ~500 °C, as evidenced in Fig. 4 by a drastic broadening of the Si $2p$ line arising from the co-existence of at least two types of silicide phases. For annealing temperatures of 550 °C and above, one observes only the single Si $2p$ contribution relevant of the CaF_2-type $CoSi_2$ phase.

Co $2p_{3/2}$ core line intensity has been measured versus polar angle Θ for several 90-Å-thick $CoSi_x$ silicide layers, in the $1<x<2$ composition range, and for a fluorite-type $CoSi_2$ layer. This latter 90-Å-thick layer was co-deposited onto a room-temperature substrate and annealed at 600 °C. The polar XPD scans have been measured in the (101) plane along the $[121]_{Si}$ and $[\bar{1}21]_{Si}$ azimuthal directions of the Si(111) substrate and compared in Figs. 5 and 6. Also shown in Figs. 5 and 6 is the angular distribution of Fe $2p_{3/2}$ intensity measured on a pseudomorphic CsCl-type derived $FeSi_2$ layer epitaxially grown on Si(111), along the same azimuthal directions of the substrate. This 90-Å-thick $FeSi_2$ silicide layer was grown by Fe and Si co-deposition onto a room-temperature Si(111) substrate.[5] A Co $2p_{3/2}$ core line intensity variation measured on ε-CoSi versus polar angle (not shown) exhibits only a featureless profile, as expected for a polycrystalline layer. The most striking feature is that, along a given azimuthal direction, the main intensity maxima are observed at the same polar angles for all silicides presented in Figs. 5 and 6. It is well known that pseudomorphic CsCl-type derived $FeSi_2$ and fluorite-type $CoSi_2$ mainly grow on Si(111) with 180° (*B*-type) orientation.[2,22–24] Thus, data of Figs. 5 and 6 indicate that $CoSi_x$ layers also grow with *B*-type orientation on Si(111). For all silicides, the $[121]_{Si}$ direction is parallel to the $[121]_{Silicide}$ one and vice versa. For sake of clarity, the azimuthal directions specified in the following discussion are those of silicides. Co $2p_{3/2}$ profiles measured on the CaF_2-type $CoSi_2$ layer exhibit prominent structures centered at polar angles $\theta=0°$, $\theta\sim30°$, and $\theta\sim55°$, in the [121] direction and $\theta\sim35°$ and 70° in the opposite [121] azimuthal direction, i.e., at polar angles aligned with dense atomic rows in the (101) plane of the CaF_2 structure. CaF_2-type $CoSi_2$ and CsCl-type FeSi structures are shown in Fig. 7, along with their cut through the (101) plane. Peaks located at $\theta=0°$, $\theta\sim55°$, and $\theta\sim70°$ appear as single peaks, while more complex features are observed at $\theta\sim30°$ in the [121] direction and $\theta\sim35°$ in the [121] direction.[24] The structure centered at $\theta\sim30°$ is composed of two sharp peaks at $\theta\sim20°$ and 35° and a deep valley in between. In the opposite [121] direction, the structure centered at $\theta\sim35°$ exhibits three well-defined maxima. As noted above, along a given azimuthal direction, the Co $2p_{3/2}$ profile measured on the room-temperature grown $CoSi_x$ exhibits intensity maxima at essentially the same polar angles as for the CaF_2-type $CoSi_2$. This means that the room-temperature-grown $CoSi_x$ silicides crystallize in a cubic structure similar to that of fluorite-type $CoSi_2$ one. Yet, the marked differences between these profiles reside in intensity changes in the broad structures centered at $\theta\sim30°$ and 35°. In the [121] direction, the deep

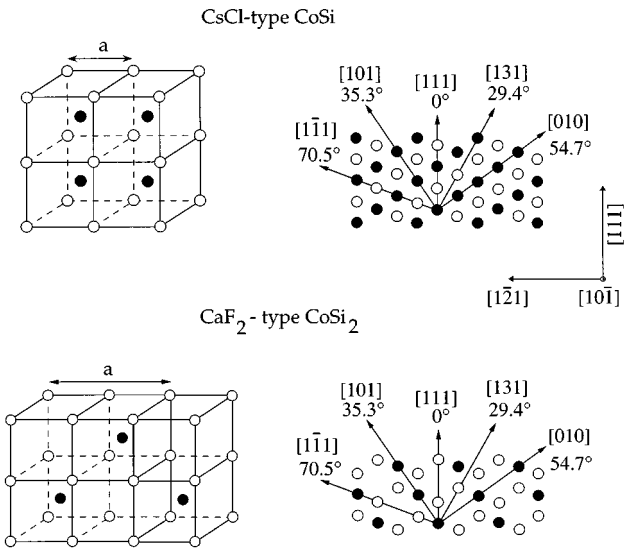

FIG. 7. CaF_2-type $CoSi_2$ and CsCl-type CoSi structures along with their cut through the (101) plane.

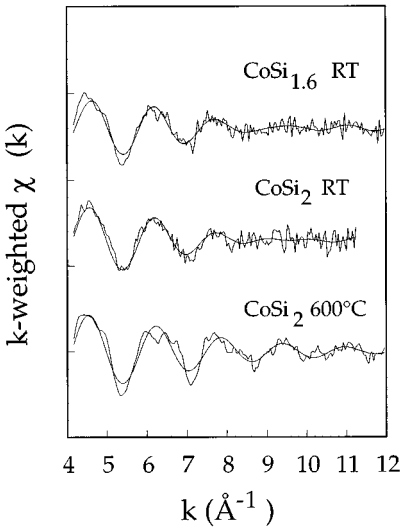

FIG. 8. k-weighted $\chi(k)$ EXAFS data recorded on 90-Å-thick fluorite-type $CoSi_2$ and room-temperature co-deposited $CoSi_{1.6}$ and $CoSi_2$, at the Co K edge. Also shown are the Fourier-filtered contribution of Si NN and Co NNN.

valley between peaks at 20° and 35° is filled for room-temperature co-deposited silicides. In the opposite [121] direction the central peak of the broad structure at $\theta \sim 35°$, aligned with the [101] crystallographic direction, has disappeared when compared to CaF_2-type $CoSi_2$. In this respect, let us consider the Fe $2p_{3/2}$ profile versus the polar angle measured on a metastable $FeSi_2$ layer, which also crystallizes in a cubic structure (upper curves of Figs. 5 and 6). This $FeSi_2$ structure is derived from the CsCl-type FeSi one shown in Fig. 7 by random removal of Fe atoms in order to reach the 1:2 composition. The CsCl-type FeSi structure is close to the CaF_2 one, with respect to XPD in the sense that the dense atomic rows appear at the same polar angle in both structures. The difference between profiles measured on the CsCl-type $FeSi_2$ and CaF_2-type $CoSi_2$ disilicides is also mainly reflected in intensity variations of the broad structures at $\theta \sim 30°$ and 35°. These structures are very sensitive to small diffraction condition changes, such as changes of the wavelength or changes in the nature of the scatterers, as shown in recent works.[24] However, the difference between wavelengths associated with Co $2p_{3/2}$ ($Ec = 706$ eV) and Fe $2p_{3/2}$ ($Ec = 779$ eV) photoelectrons is rather small. The difference between the shape of the structures at ~30° ([121] azimuth) and $\theta \sim 35°$ ([121] azimuth) in CaF_2-type $CoSi_2$ and $CoSi_x$ is, therefore, due to a change in crystallographic structure. At this stage, XPD data indicate that the room-temperature-grown $CoSi_x$ layers have a cubic structure and that it closely resembles that of CsCl-type derived $FeSi_2$. A clear-cut distinction between CaF_2-type and CsCl-type structures has been made by using a local probe as EXAFS. For instance, in a CsCl-type structure, Co would be surrounded by Co scatterers at distances of ~2.6–2.7 Å, while the closest Co scatterers are located at ~3.8 Å from the emitter in the CaF_2-type structure. EXAFS measurements at the Co K edge have been performed on $CoSi_x$ and fluorite-type $CoSi_2$ layers.

The EXAFS data have been analyzed using the software of Ref. 25. Figure 8 shows the experimental $k\chi(k)$ data recorded at the Co K edge on two epitaxial $CoSi_x$ and fluorite-type $CoSi_2$ layers. $CoSi_x$ with compositions $CoSi_{1.6}$ and $CoSi_2$ have been analyzed. These data are presented after background subtraction and normalization to the edge jump. Figure 9 displays the Fourier transforms (FT) between 3 and 12 Å^{-1} of the k^2-weighted data. Bulk $CoSi_2$ crystallizes in the CaF_2 structure, with a unit-cell length of 5.368 Å.[11] Co atoms are surrounded by 8 first-shell Si neighbors at a distance of 2.324 Å and 12 second-shell Co neighbors at 3.794 Å. These two neighbor shells are clearly visible in the FT in Fig. 9 (bottom spectrum), which is relevant to high-temperature annealed $CoSi_2$. In contrast with CaF_2-type $CoSi_2$, the first neighbor's contribution in $CoSi_x$ silicide is mainly composed of two subshells, as shown in the Fourier-transform spectra of Fig. 9. These subshells are attributed to

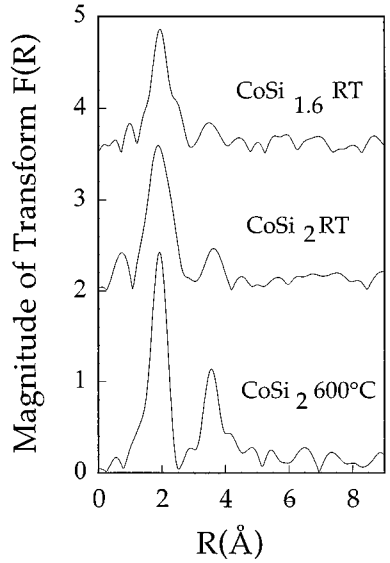

FIG. 9. Fourier-transform magnitude $F(R)$ of Co EXAFS for a 90-Å-thick fluorite-type $CoSi_2$ and room-temperature co-deposited $CoSi_{1.6}$ and $CoSi_2$.

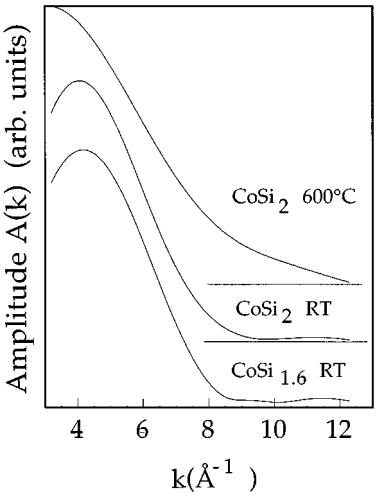

FIG. 10. Amplitude functions $A(k)$ of the Fourier-filtered contribution of Si NN and Co NNN for the 90-Å-thick fluorite-type $CoSi_2$ and room-temperature co-deposited $CoSi_{1.6}$ and $CoSi_2$.

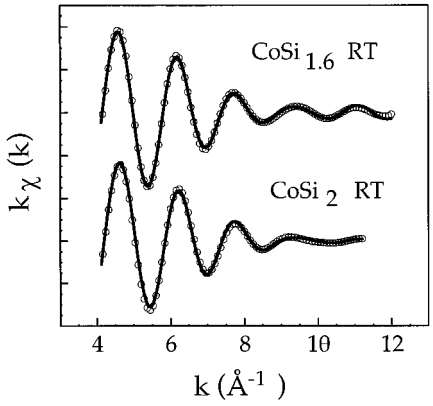

FIG. 11. Representative fits (full line) to Si NN and Co NNN Fourier-filtered signal (circles) for 90-Å-thick fluorite-type $CoSi_2$ and room-temperature co-deposited $CoSi_{1.6}$ and $CoSi_2$.

Si nearest neighbors (NN) and Co next-nearest neighbors (NNN). The presence of two subshells can be clearly evidenced, using the beat node method.[26,27] Figure 10 shows the Fourier filtered amplitude $A(k)$ of the first main peak in the Fourier transform, as a function of the electron wave vector k. For CaF_2-type $CoSi_2$ (upper curve), $A(k)$ decreases continuously, as expected for a single nearest-neighbor environment, while it exhibits a minimum at about 10 $Å^{-1}$ for RT grown $CoSi_{1.6}$ and $CoSi_2$. This technique, described in Ref. 5, allows the determination of the difference between Co-Si and Co-Co bond lengths. This difference is found to be $\sim 0.33 \pm 0.04$ Å for $CoSi_{1.6}$ and 0.34 ± 0.04 Å for $CoSi_2$. The most striking feature here is that these two subshells are observed in Fig. 9, even at the 1:2 composition. A further inspection of the Fourier-transform spectra reveals that the third-coordination shell (Co-Co-bonds) contribution is clearly visible at ~ 3.8 Å in $CoSi_{1.6}$ and $CoSi_2$ spectra. This confirms the conclusions drawn from LEED and XPD measurements, i.e., that for these compositions, Co atoms reside in a well-defined cubic environment.

The Fourier-filtered contribution of NN and NNN peaks are superimposed on the experimental data in Fig. 8. They have been simulated in the single-scattering formalism, using experimental ($CoSi_2$ and Co metal) phase shifts and backscattering amplitudes. The phase shifts and backscattering amplitudes extracted from $CoSi_2$ have been used in the calculations for the Co-Si pair, while those extracted from Co metal data have been used for the Co-Co pair. The results of the simulations along with that of the beat node method are summarized in Table I. Figure 11 shows filtered EXAFS data (dots) and fits (full line) for room-temperature grown $CoSi_2$ and $CoSi_{1.6}$. $CoSi_x$ Fourier-filtered spectra are well reproduced, assuming Si neighbors at $R_1 \sim 2.33$–2.34 Å and Co atoms at $R_2 \sim 2.67$–2.68 Å. $\Delta R = R_2 - R_1$ values of 0.33–0.34 Å given by the beat node method are in very good agreement with the value deduced from the simulations. $CoSi_2$ ($CoSi_{1.6}$) spectrum is well accounted for by 8 Si NN atoms and 3 (4) Co NNN atoms.

The NN Co-Si and NNN Co-Co bond lengths deduced from EXAFS measurements are consistent with a $CoSi_x$ silicide structure close to that of pseudomorphic $FeSi_x$ silicide, namely, a CsCl-derived structure. NNN Co-Co bond lengths of about 2.68 Å reveals that $CoSi_{1.6}$ and $CoSi_2$ lattice parameters ($a \sim 2.68$ Å) are smaller than that measured on CsCl-type CoSi ($a = 2.74$ Å).[12] Similar a lattice parameter and bond length increase versus a metal content increase was also found in $FeSi_x$ silicides. Pseudomorphic FeSi and $FeSi_2$

TABLE I. Structural parameters deduced from the analysis of EXAFS spectra recorded at the Co K edge from co-deposited cobalt silicides epitaxially grown on Si(111). $\Delta\sigma$ is related to Co-Si and and Co-Co bonds in $CoSi_2$ and Co metal, respectively. In the last column, ΔR_{BN} is the difference between the NNN Co-Co and NN Co-Si bond lengths, determined using the beat node method.

	Pair	R (Å)	N	$\Delta\sigma$ (Å)	ΔR_{BN} (Å)
$CoSi_2$					
(annealed at 600 °C)	Co-Si	2.33±0.02	8 ±0.5	0	
90 Å					
$CoSi_2$					
(RT deposited)	Co-Si	2.34±0.02	8 ±0.5	0.04	0.34±0.04
90 Å	Co-Co	2.68±0.02	3.1±1.0	0.05	
$CoSi_x$ ($x \approx 1.6$)					
(RT deposited)	Co-Si	2.34±0.02	8 ±0.5	0.06	0.33±0.04
90 Å	Co-Co	2.67±0.02	4.0±1.0	0.05	

have lattice parameters of $a=2.77$ and 2.70 Å, respectively.[3] Fe-Fe bond lengths are significantly reduced in $FeSi_2$, with respect to FeSi. Such a decrease has been confirmed by EXAFS measurements at the Fe K edge.[5] NNN Fe-Fe bond lengths of 2.75 and 2.69 Å were measured in FeSi and $FeSi_2$, respectively. A first-neighbor Co-Co bond-length reduction of the same order of magnitude is observed in the present experiments. Furthermore, Si NN and Co NNN atom coordination numbers deduced from the simulations agree also very well with a structure derived from the CsCl-type CoSi one. $CoSi_{1.6}$ and $CoSi_2$ structures are thus seen as a CoSi one in which 38% and 50% Co atoms are randomly removed, respectively. In a CsCl-type CoSi structure, Co atoms are bound to 8 Si NN and 6 Co NNN atoms. The number of Co NNN is reduced down to the mean value of 3 in a $CoSi_2$, as experimentally observed. Therefore, at a $CoSi_2$ composition, the conservation of stoichiometry requires that the number of Co atoms at ~3.84 Å must be lower in this CsCl-derived structure than in the fluorite one.

Then, a further argument for the formation of $CoSi_x$ with defected CsCl-type CoSi is given by the analysis of the third-coordination shell composed of Co atoms located at ~3.84 Å from the emitter. If, indeed, a $CoSi_x$ silicide structure is derived from a CsCl-type CoSi one, the number of Co atoms in the third-coordination shell would also decrease when the composition evolves from CoSi to $CoSi_2$. In this model, Co atoms are removed at random in all coordination shells. Fourier filtered spectra of Fig. 9 show a significant decrease of the peak at ~3.6 Å in $CoSi_x$, with respect to that in fluorite $CoSi_2$. This decrease could be attributed either to a loss of local order or to a lack of Co backscatterers. However, before any treatment of the Fourier-filtered contribution of the third-coordination shell, one must keep in mind that several multiple-scattering (MS) paths have a length close to that of the single-scattering (SS) Co-Co path and, thus, should be taken into account in the simulations. Thus, the *ab initio* multiple-scattering x-ray-absorption code FEFF (Refs. 28 and 29) was used to perform XAFS calculations including SS and MS paths around 3.8 Å. In a perfect $CoSi_2$ crystal, three double-scattering paths contribute to the peak located at ~3.6–3.8 Å in the FT: the first one called DS_1 (Co-Si-Si-Co) has a degeneracy of 24, the second one, DS_2 (Co-Si-Si-Co), has a degeneracy of 24 and the third one, DS_3 (Co-Co-Si-Co), has a degeneracy of 48. SS and DS paths are sketched in Fig. 12. These paths contribute as bond lengths of 3.66 Å (DS_1) and 4.22 Å (DS_2 and DS_3). The weighted magnitude of SS, DS_1, DS_2, and DS_3 are plotted versus wave vector k in Fig. 13. Similar calculations have been performed for a strained $CoSi_2$ layer. Indeed, when epitaxially grown on Si(111), $CoSi_2$ can be under lateral strain, due to the lattice mismatch of $\sim -1.2\%$. Only minor changes with respect to perfect cubic $CoSi_2$ are detected, as far as scattering amplitudes are concerned. The MS process has generally a smaller contribution to the total signal than the SS one. Nevertheless, it strongly depends on k. The DS_1 and DS_2 paths have an amplitude close to zero for k values higher than 6 $Å^{-1}$ while DS_3 path still has a significant contribution at high k values. However, the damping due to the Debye-Waller factors is not taken into account in these curves. The Debye-Waller factor is significantly higher in the three-legs path making the DS_3 contribution also negligible

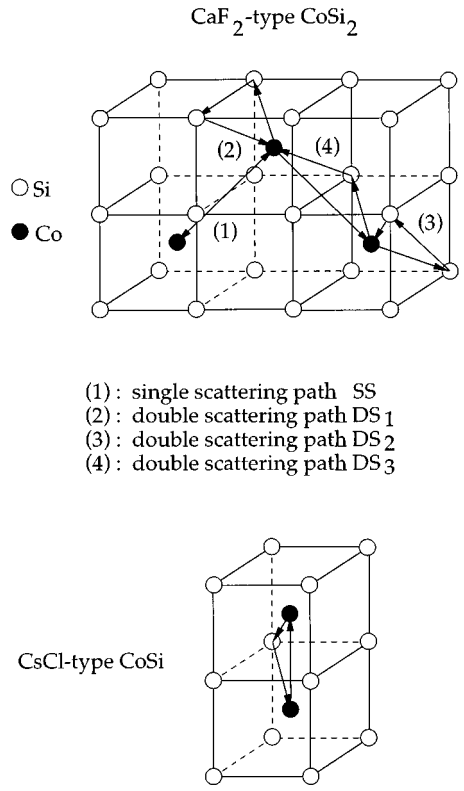

FIG. 12. A sketch of single-scattering and double-scattering paths in fluorite-type $CoSi_2$ and CsCl-type CoSi, which contribute to the peak at ~3.6–3.8 Å in the Fourier-transform spectra of Fig. 9.

above 6 $Å^{-1}$, as compared to the SS one. In the CsCl-type CoSi structure, an additional Co-Co-Si-Co (~3.66 Å) twelvefold degenerated path must be considered, as shown in Fig. 12. Nevertheless, in $CoSi_{1.6}$ and $CoSi_2$, this degeneracy decreases down to 8 or 6, making again these additional paths to contribute only weakly to the EXAFS signal. Therefore, the Fourier-filtered contribution of second- and third-coordination shells were simulated in the single-scattering formalism in the 6–13 $Å^{-1}$, for CaF_2-type $CoSi_2$ and room-

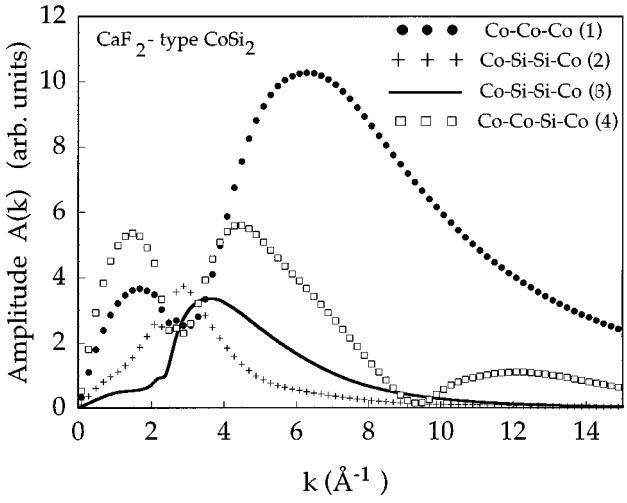

FIG. 13. Weighted magnitude of single-scattering and double-scattering paths shown in Fig. 12, as a function of wave vector k.

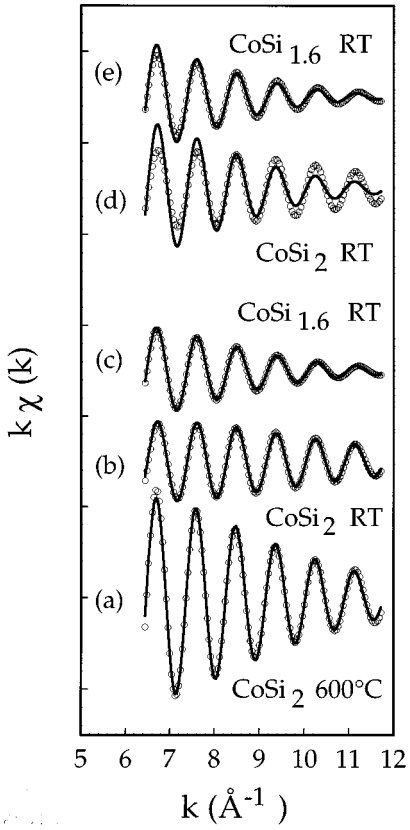

FIG. 14. Representative fits (full line) to the third-coordination shell Fourier-filtered signal (circles) for 90-Å-thick fluorite-type $CoSi_2$ (a) and room-temperature co-deposited $CoSi_2$ (b) and $CoSi_{1.6}$ (c). Also shown are the fits for room temperature co-deposited $CoSi_2$ (d) and $CoSi_{1.6}$ (e) performed assuming 12 Co backscatterers.

temperature grown $CoSi_{1.6}$ and $CoSi_2$, respectively. Experimental spectra were simulated using theoretical phase shifts and backscattering amplitudes.[28,29] Figure 14 shows filtered EXAFS data (dots) and fits (full line) for CaF_2-type $CoSi_2$ and room-temperature grown $CoSi_2$ and $CoSi_{1.6}$. The results of the simulations are summarized in Table II. Simulations reveal that Co atoms are bound to 12 Co at $R_3 \sim 3.84 \pm 0.04$ Å in the fluorite-type $CoSi_2$ annealed at 600 °C. Such a bond length, larger than that of a bulk CaF_2-type $CoSi_2$ structure, is very close to the translation periodicity (~3.84 Å) of the Si(111) surface. This would suggest that the high-temperature annealed $CoSi_2$ layer is rather well matched to the Si(111) substrate, i.e., it is laterally strained. This is surprising since it has been recently demonstrated that CaF_2-type $CoSi_2$ layer with comparable thickness annealed at 600–650 °C are fully relaxed instead.[30] Thus, third-coordination shell bond length R_3 deduced from EXAFS seems overestimated by about 1%. The R_3 bond lengths, shown in Table II for RT $CoSi_2$ and $CoSi_{1.6}$, would have to be reduced, accordingly. In doing so, these bond lengths would be of 3.80 Å (RT $CoSi_2$) and 3.78 Å (RT $CoSi_{1.6}$), as expected for cubic CsCl-type structure with second-coordination shell bond length of 2.68 Å (RT $CoSi_2$) and 2.67 Å (RT $CoSi_{1.6}$). Furthermore, simulations of Fig. 14 clearly demonstrate that the important decrease of the FT peak at 3.6–3.8 Å in co-deposited silicides, with respect to that of fluorite-type $CoSi_2$, cannot be assigned to a loss of local order, only. Indeed, any attempt to simulate these spectra with 12 Co has failed. Thus, the damping of the FT peak is mainly due to a true change in the Co number of third-shell neighbors, associated with a change in crystal structure. The coordination number deduced from the simulation is of 7 in $CoSi_{1.6}$ and of 5 in $CoSi_2$. At $CoSi_{1.6}$ and $CoSi_2$ compositions, third-shell mean coordination numbers of 8 and 6 are expected in a defected CsCl-type CoSi, in rather good agreement with experimental results summarized in Table II. This lends strong support to random (defected CsCl-type), as opposed to ordered (CaF_2-type) occupation of the Co sites. However, because of the limited accuracy of third-shell coordination-number determinations in EXAFS, some deviation from perfect random distribution, with a preferential occupation of third-shell Co sites, cannot be ruled out and might be evidenced by x-ray-diffraction experiments.

TABLE II. Structural parameters deduced from the analysis of the third-coordination shell Fourier-filtered EXAFS spectra recorded at the Co K edge from co-deposited cobalt silicides and CaF_2-type $CoSi_2$ layers epitaxially grown on Si(111).

	Pair	R (Å)	N	σ (Å)
90-Å $CoSi_2$ (annealed at 600 °C)	Co-Co	3.84±0.04	12±3	0.08
90-Å $CoSi_2$ (RT deposited)	Co-Co	3.84±0.04	5±3	0.06
90-Å $CoSi_{1.6}$ (RT deposited)	Co-Co	3.82±0.04	7±3	0.11

IV. CONCLUSIONS

In summary, XPD profiles, Co-Si and Co-Co bond lengths deduced from EXAFS data as well as Si $2p$ core level, and valence-band photoemission demonstrate that pseudomorphic $CoSi_x$ ($1 \leqslant x \leqslant 2$) silicides grown by room-temperature co-deposition crystallize basically in a CsCl-type structure with randomly distributed Co vacancies very similar to that of pseudomorphic $FeSi_x$ silicides. In particular, it is shown that $CoSi_2$ can adopt a crystal structure different from that of the stable CaF_2-type $CoSi_2$, despite the small lattice mismatch (−1.2%) of this latter structure, with respect to Si. The growth of this $CoSi_2$ phase cannot be explained by its greater stability in the form of the films, as found for $FeSi_2$, but most likely results from kinetic factors.

[1] H. von Känel, K. A. Mäder, E. Müller, N. Onda, and H. Sirringhaus, Phys. Rev. B **45**, 13 807 (1992).

[2] N. Onda, J. Henz, E. Müller, K. A. Mäder, and H. von Känel, Appl. Surf. Sci. **56-58**, 421 (1992).

[3] N. Onda, H. Sirringhaus, S. Goncalves-Conto, C. Schwartz, E. Müller-Gubler, and H. von Känel, in *Evolution of Surface and Thin Film Microstructure*, edited by H. A. Atwater, E. Chason, M. Grabow, and M. Lagally, MRS Symposia Proceedings No. 280 (Materials Research Society, Pittsburgh, 1993), p. 581.

[4] U. Kafader, M. H. Tuilier, C. Pirri, P. Wetzel, G. Gewinner, D.

Bolmont, O. Heckmann, D. Chanderis, and H. Magnan, Europhys. Lett. **22**, 529 (1993).
[5] C. Pirri, M. H. Tuilier, P. Wetzel, S. Hong, D. Bolmont, G. Gewinner, R. Cortès, and O. Heckmann, Phys. Rev. B **51**, 2302 (1995).
[6] X. W. Lin, M. Behar, J. Desimoni, H. Bernas, J. Washburn, and Z. Liliental-Weber, Appl. Phys. Lett. **63**, 105 (1993).
[7] N. Jedrecy, A. Waldhauer, M. Sauvage-Simkin, R. Pinchaux, and Y. Zheng, Phys. Rev. B **49**, 4725 (1994).
[8] H. von Känel, R. Stalder, H. Sirringhaus, N. Onda, and J. Henz, Appl. Surf. Sci. **43**, 196 (1991).
[9] A. L. Vazquez de Parga, J. De la Figuera, C. Ocal, and R. Miranda, Europhys. Lett. **18**, 595 (1992).
[10] X. Wallart, J. P. Nys, and C. Tételin, Phys. Rev. B **49**, 5714 (1994).
[11] P. Villars and L. D. Calvert, *Pearson's Handbook of Crystallographic Data for Intermetallic Phases* (American Society for Metals, Metals Park, 1985).
[12] H. von Känel, C. Schwartz, S. Goncalves-Conto, E. Müller, L. Miglio, F. Tavazza, and G. Malegori, Phys. Rev. Lett. **74**, 1163 (1995).
[13] R. T. Tung and F. Schrey, Appl. Phys. Lett. **54**, 852 (1989).
[14] H. von Känel, Mater. Sci. Rep. **8**, 193 (1992), and references therein.
[15] L. Haderbache, P. Wetzel, C. Pirri, J. C. Peruchetti, D. Bolmont, and G. Gewinner, Phys. Rev. B **39**, 1422 (1989).
[16] L. Haderbache, P. Wetzel, C. Pirri, J. C. Peruchetti, D. Bolmont, and G. Gewinner, Thin Solid Films **184**, 365 (1990).
[17] C. Pirri, J. C. Peruchetti, G. Gewinner, and D. Bolmont, Solid State Commun. **57**, 361 (1986).
[18] S. J. Oh, J. W. Allen, and J. M. Lawrence, Phys. Rev. B **35**, 2267 (1987).
[19] W. Speier, E. v. Leuken, J. C. Fuggle, D. D. Sarma, L. Kumar, B. Dauth, and K. H. J. Buschow, Phys. Rev. B **39**, 6008 (1989).
[20] C. Pirri, J. C. Peruchetti, G. Gewinner, and J. Derrien, Phys. Rev. B **28**, 3391 (1984).
[21] J. Tersoff and D. R. Hamman, Phys. Rev. B **28**, 1168 (1983).
[22] R. T. Tung, J. M. Gibson, and J. M. Poate, Phys. Rev. Lett. **50**, 429 (1983).
[23] U. Kafader, C. Pirri, P. Wetzel, and G. Gewinner, Appl. Surf. Sci. **64**, 297 (1993).
[24] S. Hong, C. Pirri, P. Wetzel, D. Bolmont, and G. Gewinner, Appl. Surf. Sci. **90**, 65 (1995).
[25] A. Michalovicz, *Logiciels pour la Chimie*, edited by Société Francaise de Chimie (Publisher, Paris, 1991), p. 102.
[26] G. Martens, P. Robe, N. Schwentner, and A. Werner, Phys. Rev. Lett. **39**, 1411 (1977).
[27] A. Balzarotti, F. Comin, L. Incoccia, S. Mobilio, M. Piacentini, and A. Savoia, in *Inner-shell and X-ray Physics of Atoms and Solids*, edited by D. J. Fabian, H. Kleinpoppen, and L. M. Watson (Plenum, New York, 1981), p. 723.
[28] J. Mustre de Leon, J. J. Rehr, S. I. Zabrinsky, and R. C. Albers, Phys. Rev. B **44**, 4146 (1991).
[29] J. J. Rehr, R. C. Albers, and S. I. Zabrinsky, Phys. Rev. Lett. **59**, 3397 (1992).
[30] R. Stalder, H. Sirringhaus, N. Onda, and H. von Känel, Appl. Phys. Lett. **59**, 1960 (1991).